

**MICROFABRICATION OF ROTATIONALLY SYMMETRIC  
COMPONENTS THROUGH DRY MICRO ELECTRIC  
DISCHARGE TURNING**

**HARISH KUMAR**



**DEPARTMENT OF MECHANICAL ENGINEERING  
INDIAN INSTITUTE OF TECHNOLOGY DELHI  
MARCH 2024**

**© Indian Institute of Technology Delhi, New Delhi 2024**

**MICROFABRICATION OF ROTATIONALLY SYMMETRIC  
COMPONENTS THROUGH DRY MICRO ELECTRIC  
DISCHARGE TURNING**

by

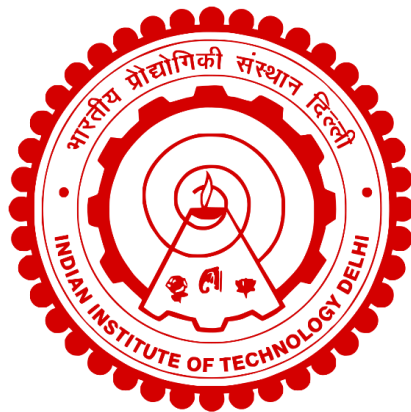
**HARISH KUMAR**

**DEPARTMENT OF MECHANICAL ENGINEERING**

submitted

in fulfilment of the requirements of the degree of **Doctor of Philosophy**

to the



**INDIAN INSTITUTE OF TECHNOLOGY DELHI**

**MARCH 2024**

This thesis is devoted to the  
Supreme deity of wisdom and transformation

“Lord Shiva”



ॐ नमः शिवाय गुरवे

सच्चिदानंदमूर्तये।

निष्पापाय शान्ताय निरालम्बाय तेजसे॥

OM NAMAH SHIVAYA GURAVE  
SATCHIDANANDA MURTAYE  
NISHPAPAYA SHANTAYA NIRALAMBAYA TEJASE

Lord Shiva is the supreme teacher, the source of knowledge and  
wisdom for the pursuit of truth and inner peace in the journey towards  
acquiring knowledge and enlightenment

## **CERTIFICATE**

This is to certify that the work contained in the thesis entitled “**Microfabrication of Rotationally Symmetric Components Through Dry Micro Electric Discharge Turning**” submitted by **Mr. Harish Kumar** has been carried out at the Indian Institute of Technology Delhi, for the award of the degree of **Doctor of Philosophy**, in the Department of Mechanical Engineering is a record of bonafide original research work carried out by him under my guidance and supervision.

The results contained in it have not been submitted in part or full to any other institution or university for the award of any degree.

**Dr. Sunil Jha**

Professor

Department of Mechanical Engineering

Indian Institute of Technology Delhi

## ACKNOWLEDGMENTS

I am filled with profound gratitude for "Maa Gayatri," whose spiritual guidance and unwavering support have given me the inner strength to overcome the challenges encountered on this journey. Her blessings have offered a remarkable opportunity to delve into the complexities of nature and make meaningful contributions to the global knowledge base. Also, a perpetual wellspring of inspiration, and the thought of her during difficult moments has illuminated my thinking and motivated me to successfully accomplish this endeavour.

I would like to express my sincere gratitude to my supervisor, *Prof. Sunil Jha*, for their exceptional expertise, patience, and invaluable insights, which have significantly influenced me to complete this thesis. His mentorship and guidance on the subject, coupled with constructive criticism, have played a vital role in honing my research and academic abilities. His support has encouraged me to explore various dimensions of research and recognize the significance of diligence and a thoughtful investigative approach. I deeply appreciate the trust they have bestowed upon me throughout this academic journey.

Next, I would like to express my gratitude to my dear parents, *Mr. Kanchhi Singh* and *Mrs. Sushma Devi* for allowing me to select my career path and backing my aspirations. Your limitless affection and confidence in my abilities have been the impetus propelling me in the pursuit of knowledge. Your sacrifices and understanding have been a constant source of sustenance during numerous hours of unwavering dedication.

I express my gratitude to my SRC chairman *Prof. Sudarsan Ghosh*, who constantly motivated me through his positive suggestions during SRC presentations. I am also thankful to other members of my SRC committee, *Prof. P.M Pandey*, *Prof. Gufran S. Khan*, and *Dr. Prithviraj Mukhopadhyay*, who provided valuable inputs in improving my research work. Furthermore, I would like to thank *Dr. Tribeni Roy* of Birla Institute of Technology, Pilani for continuous encouragement in the subject matter and other innovative areas. Their contributions have been instrumental in shaping my research journey. A special thanks to the lab technical staff, *Mr. Tulsi Ram*, and *Mr. Paras Gupta*, whose technical expertise and assistance ensured the smooth execution of experiments and completing the work on time.

I am thankful to the Department of Science and Technology (DST), New Delhi, India, for their financial support, to develop my experimental setup under project no. DST/TSG/NTS/2015/114-C entitled "Advanced CNC micromachining system with integrated micro tool manufacturing" has been instrumental in successfully completing my research work. I further

thankfully acknowledge the Department of Science and Technology (DST), New Delhi, India, for their financial support as an INSPIRE Fellowship (IF-160098) during my Ph.D. tenure.

I sincerely thank my seniors *Dr. Faiz Iqbal, Dr. Dilshad Ahmad Khan, and Dr. Zafar Alam*, for providing motivational support and technical know-how throughout my research. I am also thankful to my colleague *Dr. Ashish Kr. Sahu, Dr. Jitin Malhotra, Dr. Hardik A. Patel, Mr Onkar Chawla, Mr. Tarun Verma, Mr. Nitin Patel, Mr. Aman Nohwal, Mr. Sudhanshu Maurya, Mr. Deepak Kumar* and friends from Automation Lab., *Mr. Navdeep Singh, Mr. Arun Kumar, and Mr. Aman Kumar*, whose presence has made the challenges more manageable and the triumphs more meaningful.

I express my heartfelt gratitude to my in-laws, *Mr. Dinesh Pal Singh Shishodia and Mrs. Kamlesh Shishodia*, for their blessings, motivation, and constant support throughout this period. Additionally, I am grateful to my younger brothers, *Kaushal Kumar Chauhan, and Vikash Kumar Chauhan*, as well as my sister, *Shivani*, for generously sharing their time and ensuring I remain stress-free and able to enjoy life. Their support has enabled me to maintain focus on my work consistently.

I deeply appreciate the unwavering love and support of my wife, *Mrs. Vandana Shishodia*. Her kind cooperation and immense inspiration have been constant companions throughout our journey together, which began even before my joining at IITD. Without her steadfast support, this research contribution would have never come to fruition, and mere words cannot adequately express the depth of gratitude I hold for her. I extend my affection to my sons, *Shaurya Chauhan, and Shiva Chauhan*, for their consistent support and understanding during my Ph.D. journey. Their presence infused my life with happiness and calmness, motivating me to strive for success.

Last but not least, I am thankful to everyone at IIT Delhi and outside who encouraged me directly or indirectly to complete this work.

Harish Kumar

## ABSTRACT

Micromachining is a foundational technology for creating miniature components measuring less than 500  $\mu\text{m}$ . In today's manufacturing landscape, micromachining holds increasing significance due to the ongoing trend of miniaturizing industrial products. Tool-based micromachining methods, including  $\mu$ -turning,  $\mu$ -grinding,  $\mu$ -EDM, and  $\mu$ -ECM, offer a range of advantages encompassing productivity, efficiency, adaptability, and cost-effectiveness. Meeting the current industrial demand for high dimensional accuracy and superior surface quality is of utmost importance. Within this domain,  $\mu$ -EDM emerges as an important method for the economical production of intricate microfeatures characterized by exceptional precision.

The development of a dry  $\mu$ EDM system has significantly improved the environmental sustainability of the machining process. A customized pulse generator, fine-tuned for  $\mu$ EDM, ensures precise control of electrical parameters. The indigenously developed electrically isolated EDM spindle, with a runout error of less than 10  $\mu\text{m}$ , enables accurate microelectrode fabrication. This setup supports dry  $\mu$ EDM drilling, milling, and turning operations, and an integrated camera enhances the in-situ measurement capabilities. Brass microelectrodes having aspect ratios of more than 40 have been fabricated. The minimum diameter of the fabricated microelectrode was  $\sim 85\mu\text{m}$ .

However, the issue of high tool wear rates necessitates the on-machine fabrication of high aspect-ratio microelectrodes. These microelectrodes play a crucial role in creating micro holes and channels during  $\mu$ EDM drilling and milling operations. The central challenge in  $\mu$ EDM lies in fabricating high aspect-ratio microelectrodes that combine high dimensional accuracy. This study explores the realm of microelectrode fabrication through dry  $\mu$ EDM, deploying five distinct machining strategies. These strategies significantly reduce the taper issue, including stationary block electric discharge turning (SB-EDT), moving block electric discharge turning (MB-EDT), and their combinations. MB-EDT<sub>d</sub> creates microelectrodes with nearly zero taper and a remarkable surface finish of 2.04  $\mu\text{m}$ . Additionally, the research highlights the achievement of the highest material removal rate through MB-EDT<sub>d</sub>, culminating in microelectrodes with an average diameter of 428  $\mu\text{m}$ . The study's comprehensive approach encompasses SEM micrographs and surface finish analyses of various parameters, such as varying discharge currents and linear feed, on the microelectrode fabrication.

Further, a parametric study delves into the impact of non-electrical parameters on Material Removal Rate (MRR) and Surface Roughness ( $R_a$ ) in microelectrode fabrication using dry

$\mu$ EDT. A robust statistical model was developed and validated within a 95% confidence interval, offering a reliable tool for predicting and controlling the fabrication process. The model reveals a strong correlation between the response variables and process factors, with  $R_{adjusted}^2$  values of 94.82 for MRR and 92.55 for  $R_a$ , emphasizing its efficacy in quantifying the relationship between non-electrical parameters and microelectrode characteristics. The research underscores the significant influence of specific non-electrical parameters, with dielectric pressure emerging as a primary contributor to MRR (57.78%) and  $R_a$  (42.77%). Spindle rotation speed and block linear feed also affect these characteristics, though to a lesser degree, providing insights for process optimization. Employing a multi-objective genetic algorithm for optimization led to the identification of optimal parameters: a spindle rotation speed of 412 rpm, a block linear feed rate of 7.36 mm/sec, and a dielectric pressure of 6.4 bar. Under these conditions, the study achieved an impressive MRR of 0.0087  $\mu\text{m}^3/\text{min}$  and a low  $R_a$  of 0.6138  $\mu\text{m}$ , demonstrating the viability of producing high-quality microelectrodes through dry  $\mu$ EDT.

The comprehensive comparative analysis delves into the influence of various gaseous dielectrics on microelectrode fabrication, exploring compressed air, oxygen, nitrogen, argon, and mixed dielectrics like air-argon and oxygen-argon. The research also delves into the impact of discharge energy on surface morphology, suggesting optimal dielectric selection for distinct machining purposes. Oxygen-argon dielectric emerges as advantageous for high material removal rates, making it ideal for material removal processes. Conversely, argon dielectric excels in finishing operations. Among all dielectrics, nitrogen consistently delivers a superior surface finish, with a surface roughness as low as 1.663  $\mu\text{m}$  during semi-finish machining. For fine surface quality in finish cuts, argon dielectric stands out with a surface finish as low as 0.765  $\mu\text{m}$ . Qualitative analysis using XMCT reveals variations in material density on microelectrode surfaces, providing valuable insights into machined surface characteristics for different dielectrics, such as rough, semi-finish, and finish cuts. The research underscores the relationship between discharge energy and recast layer thickness (RLT). Oxygen-argon dielectric exhibits the highest RLT at 6000  $\mu\text{J}$  discharge energy, measuring 65.23  $\mu\text{m}$ , while argon dielectric at 200  $\mu\text{J}$  discharge energy yields the lowest RLT at 20.33  $\mu\text{m}$ . This information aids in selecting appropriate discharge energy levels for specific machining requirements. EDAX elemental analysis reveals a connection between oxygen in the dielectric and increased oxygen and carbon percentages on the machined surface. The presence of  $\text{O}_2$  in the dielectric contributes to oxide and carbide formation on microelectrode surfaces.

Microelectrodes fabricated with oxygen and air-argon dielectric exhibit the highest weight percentages of O<sub>2</sub> and carbon elements. This knowledge guides dielectric selection to control the surface chemistry of the machined surface.

A hydrophobic surface has been developed on Al-6061 alloy using two gaseous dielectric mediums using a dry  $\mu$ EDM milling process. It reveals that machining in an oxygen environment yields an uneven surface with a higher S<sub>a</sub> value while machining in argon results in a smoother, more hydrophobic surface with uniform micro textures. Chemical analyses, including EDAX and XRD, show shifts in composition and the presence of hydrophilic compounds, particularly in oxygen-machined samples with a higher oxide count. XPS analysis highlights oxidation, with a broadened aluminum oxide peak and a shift towards higher binding energies, contributing to reduced contact angles. Furthermore, a higher C/Al atomic ratio in argon-machined samples suggests organic compound adsorption, enhancing hydrophobicity. These findings collectively elucidate the critical role of machining environments and surface chemistry in developing hydrophobic aluminum surfaces, offering valuable insights for various applications.

**Keywords:** micromachining, dry electrical discharge machining, dry electrical discharge turning, dielectric gases, microelectrode fabrication, wettability

## सार

माइक्रोमशीनिंग 500 माइक्रोन से कम माप वाले लघु घटक बनाने की एक मूलभूत तकनीक है। आज के विनिर्माण परिदृश्य में, औद्योगिक उत्पादों को छोटा करने की चल रही प्रवृत्ति के कारण माइक्रोमशीनिंग का महत्व बढ़ रहा है। माइक्रो-टर्निंग, माइक्रो-ग्राइंडिंग, माइक्रो-ईडिम और माइक्रो-ईसीएम सहित टूल-आधारित माइक्रोमशीनिंग विधियां, उत्पादकता, दक्षता, अनुकूलनशीलता और लागत-प्रभावशीलता सहित कई प्रकार के लाभ प्रदान करती हैं। उच्च आयामी सटीकता और बेहतर सतह गुणवत्ता की वर्तमान औद्योगिक मांग को पूरा करना अत्यंत महत्वपूर्ण है। इस डोमेन के भीतर, माइक्रो ईडिम असाधारण परिशुद्धता द्वारा विशेषता जटिल माइक्रोफीचर्स के किफायती उत्पादन के लिए एक महत्वपूर्ण विधि के रूप में उभरता है।

शुष्क माइक्रो ईडिम प्रणाली के विकास ने मशीनिंग प्रक्रिया की पर्यावरणीय स्थिरता में काफी सुधार किया है। माइक्रो ईडिम के लिए फाइन-ट्यून किया गया एक अनुकूलित पल्स जनरेटर, विद्युत मापदंडों का सटीक नियंत्रण सुनिश्चित करता है। स्वदेशी रूप से विकसित विद्युत पृथक ईडीएम स्पिंडल, 10 माइक्रोन से कम की रनआउट त्रुटि के साथ, सटीक माइक्रोइलेक्ट्रोड निर्माण को सक्षम बनाता है। यह सेटअप शुष्क माइक्रो ईडिम ड्रिलिंग, मिलिंग और टर्निंग ऑपरेशन का समर्थन करता है, और एक एकीकृत कैमरा इन-सीटू माप क्षमताओं को बढ़ाता है। 40 से अधिक पहलू अनुपात वाले पीतल के माइक्रोइलेक्ट्रोड का निर्माण किया गया है। निर्मित माइक्रोइलेक्ट्रोड का न्यूनतम व्यास ~85 माइक्रोन था।

हालाँकि, उच्च उपकरण घिसाव दर के मुद्दे के कारण उच्च पहलू-अनुपात माइक्रोइलेक्ट्रोड के ऑन-मशीन निर्माण की आवश्यकता होती है। ये माइक्रोइलेक्ट्रोड माइक्रो ईडिम ड्रिलिंग और मिलिंग संचालन के दौरान सूक्ष्म छेद और चैनल बनाने में महत्वपूर्ण भूमिका निभाते हैं। माइक्रो ईडिम में केंद्रीय चुनौती उच्च पहलू-अनुपात वाले माइक्रोइलेक्ट्रोड का निर्माण करना है जो उच्च आयामी सटीकता को जोड़ते हैं। यह अध्ययन पांच अलग-अलग मशीनिंग रणनीतियों को तैनात करते हुए, शुष्क माइक्रो ईडिम के माध्यम से माइक्रोइलेक्ट्रोड निर्माण के दायरे की पड़ताल करता है। ये रणनीतियाँ टेपर समस्या को काफी हद तक कम करती हैं, जिसमें स्थिर ब्लॉक इलेक्ट्रिक डिस्चार्ज टर्निंग (एसबी-ईडीटी), मूविंग ब्लॉक इलेक्ट्रिक डिस्चार्ज टर्निंग (एमबी-ईडीटी), और उनके संयोजन शामिल हैं। एमबी-ईडीटीडी लगभग शून्य टेपर और 2.04 माइक्रोन की उल्लेखनीय सतह फिनिश के साथ माइक्रोइलेक्ट्रोड बनाता है। इसके अतिरिक्त, अनुसंधान एमबी-ईडीटीडी के माध्यम से उच्चतम सामग्री निष्कासन दर की उपलब्धि पर प्रकाश डालता है, जिसका समापन 428 माइक्रोन के औसत व्यास वाले माइक्रोइलेक्ट्रोड में होता है। अध्ययन के व्यापक दृष्टिकोण में माइक्रोइलेक्ट्रोड निर्माण पर अलग-अलग डिस्चार्ज धाराओं और रैखिक फ़ीड जैसे विभिन्न मापदंडों के एसईएम माइक्रोग्राफ और सतही फिनिश विश्लेषण शामिल हैं।

इसके अलावा, एक पैरामीट्रिक अध्ययन शुष्क माइक्रो ईडिटी का उपयोग करके माइक्रोइलेक्ट्रोड निर्माण में सामग्री निष्कासन दर (एमआरआर) और सतह खुरदरापन ( $R_a$ ) पर गैर-विद्युत मापदंडों के प्रभाव का पता लगाता है। 95% विश्वास अंतराल के भीतर एक मजबूत सांख्यिकीय मॉडल विकसित और मान्य किया गया था, जो निर्माण प्रक्रिया की भविष्यवाणी और नियंत्रण के लिए एक विश्वसनीय उपकरण प्रदान करता है। मॉडल प्रतिक्रिया चर और प्रक्रिया कारकों के बीच एक मजबूत सहसंबंध को प्रकट करता है, एमआरआर के लिए 94.82 और  $R_a$  के लिए 92.55 के  $R_{adjusted}^2$  मूल्यों के साथ, गैर-विद्युत मापदंडों और माइक्रोइलेक्ट्रोड विशेषताओं के बीच संबंध को मापने में इसकी प्रभावकारिता पर जोर देता है। अनुसंधान विशिष्ट गैर-विद्युत मापदंडों के महत्वपूर्ण प्रभाव को रेखांकित करता है, जिसमें ड्राईइलेक्ट्रिक दबाव एमआरआर (57.78%) और  $R_a$  (42.77%) के प्राथमिक योगदानकर्ता के रूप में उभर रहा है। स्पिंडल रोटेशन गति और ब्लॉक रैखिक फ़ीड भी इन विशेषताओं को प्रभावित करते हैं, हालांकि कुछ हद तक, प्रक्रिया अनुकूलन के लिए अंतर्दृष्टि प्रदान करते हैं। अनुकूलन के लिए एक बहुउद्देशीय आनुवंशिक एल्गोरिदम को नियोजित करने से इष्टतम मापदंडों की पहचान हुई: 412 आरपीएम की स्पिंडल रोटेशन गति, 7.36 मिमी/सेकंड की ब्लॉक रैखिक फ़ीड दर, और 6.4 बार का ड्राईइलेक्ट्रिक दबाव। इन परिस्थितियों में, अध्ययन ने  $0.0087 \mu\text{m}^3/\text{min}$  का प्रभावशाली एमआरआर और 0.6138 माइक्रोन का निम्न  $R_a$  हासिल किया, जो शुष्क माइक्रो ईडिटी के माध्यम से उच्च गुणवत्ता वाले माइक्रोइलेक्ट्रोड के उत्पादन की व्यवहार्यता को प्रदर्शित करता है।

व्यापक तुलनात्मक विश्लेषण माइक्रोइलेक्ट्रोड निर्माण पर विभिन्न गैसीय डाइलेक्ट्रिक्स के प्रभाव का पता लगाता है, कार्बोनाइट्रोजन, ऑक्सीजन, नाइट्रोजन, आर्गन और एयर-आर्गन और ऑक्सीजन-आर्गन जैसे मिश्रित डाइलेक्ट्रिक्स की खोज करता है। यह शोध सतह मॉर्फोलॉजी पर डिस्चार्ज ऊर्जा के प्रभाव पर भी प्रकाश डालता है, जो अलग-अलग मशीनिंग उद्देश्यों के लिए इष्टतम ड्राईइलेक्ट्रिक चयन का सुझाव देता है। ऑक्सीजन-आर्गन ड्राईइलेक्ट्रिक उच्च सामग्री हटाने की दर के लिए फायदेमंद बनकर उभरता है, जो इसे सामग्री हटाने की प्रक्रियाओं के लिए आदर्श बनाता है। इसके विपरीत, आर्गन ड्राईइलेक्ट्रिक परिष्करण कार्यों में उत्कृष्टता प्राप्त करता है। सभी डाइलेक्ट्रिक्स के बीच, नाइट्रोजन लगातार बेहतर सतह फिनिश प्रदान करता है, सेमी-फिनिश मशीनिंग के दौरान सतह खुरदरापन 1.663 माइक्रोन तक कम होता है। फिनिश कट में बढ़िया सतह गुणवत्ता के लिए, आर्गन ड्राईइलेक्ट्रिक 0.765 माइक्रोन जितनी कम सतह फिनिश के साथ सामने आता है। एक्सएमसीटी का उपयोग करके गुणात्मक विश्लेषण से माइक्रोइलेक्ट्रोड सतहों पर सामग्री घनत्व में भिन्नता का पता चलता है, जो विभिन्न डाइलेक्ट्रिक्स, जैसे रफ, सेमी-फिनिश और फिनिश कट्स के लिए मशीनीकृत सतह विशेषताओं में मूल्यवान अंतर्दृष्टि प्रदान करता है। शोध डिस्चार्ज एनर्जी और रीकास्ट लेयर थिकनेस (आरएलटी) के बीच संबंध को रेखांकित करता है।

ऑक्सीजन-आर्गन डाईइलेक्ट्रिक 6000  $\mu\text{J}$  डिस्चार्ज ऊर्जा पर उच्चतम आरएलटी प्रदर्शित करता है, जिसकी माप 65.23 माइक्रोन है, जबकि 200  $\mu\text{J}$  डिस्चार्ज ऊर्जा पर आर्गन डाईइलेक्ट्रिक 20.33 माइक्रोन पर सबसे कम आरएलटी उत्पन्न करता है। यह जानकारी विशिष्ट मशीनिंग आवश्यकताओं के लिए उचित निर्वहन ऊर्जा स्तर का चयन करने में सहायता करती है। EDAX मौलिक विश्लेषण से डाईइलेक्ट्रिक में ऑक्सीजन और मशीनीकृत सतह पर बड़े हुए ऑक्सीजन और कार्बन प्रतिशत के बीच संबंध का पता चलता है। डाईइलेक्ट्रिक में  $\text{O}_2$  की उपस्थिति माइक्रोइलेक्ट्रोड सतहों पर ऑक्साइड और कार्बाइड के निर्माण में योगदान करती है। ऑक्सीजन और एयर-आर्गन डाईइलेक्ट्रिक से निर्मित माइक्रोइलेक्ट्रोड ऑक्सीजन और कार्बन तत्वों का उच्चतम वजन प्रतिशत प्रदर्शित करते हैं। यह ज्ञान मशीनीकृत सतह की सतह रसायन विज्ञान को नियंत्रित करने के लिए डाईइलेक्ट्रिक चयन का मार्गदर्शन करता है।

शुष्क माइक्रो ईडिम मिलिंग प्रक्रिया का उपयोग करके दो गैसीय डाईइलेक्ट्रिक माध्यमों का उपयोग करके AI-6061 मिश्र धातु पर एक हाइड्रोफोबिक सतह विकसित की गई है। इससे पता चलता है कि ऑक्सीजन वातावरण में मशीनिंग से उच्च  $S_a$  मान के साथ एक असमान सतह प्राप्त होती है जबकि आर्गन में मशीनिंग से समान सूक्ष्म बनावट के साथ स्मूदर, अधिक हाइड्रोफोबिक सतह प्राप्त होती है। EDAX और XRD सहित रासायनिक विश्लेषण, संरचना में बदलाव और हाइड्रोफिलिक यौगिकों की उपस्थिति दिखाते हैं, विशेष रूप से उच्च ऑक्साइड गिनती वाले ऑक्सीजन-मशीनीकृत नमूनों में। एक्सपीएस विश्लेषण व्यापक एल्यूमीनियम ऑक्साइड शिखर और उच्च बाध्यकारी ऊर्जा की ओर बदलाव के साथ ऑक्सीकरण पर प्रकाश डालता है, जो कम संपर्क कोणों में योगदान देता है। इसके अलावा, आर्गन-मशीनीकृत नमूनों में उच्च C/AI परमाणु अनुपात कार्बनिक यौगिक सोखने का सुझाव देता है, जिससे हाइड्रोफोबिसिटी बढ़ती है। ये निष्कर्ष सामूहिक रूप से हाइड्रोफोबिक एल्यूमीनियम सतहों को विकसित करने में मशीनिंग वातावरण और सतह रसायन विज्ञान की महत्वपूर्ण भूमिका को स्पष्ट करते हैं, जो विभिन्न अनुप्रयोगों के लिए मूल्यवान अंतर्दृष्टि प्रदान करते हैं।

**कीवर्ड:** माइक्रोमशीनिंग, डाई इलेक्ट्रिकल डिस्चार्ज मशीनिंग, डाई इलेक्ट्रिकल डिस्चार्ज टर्निंग, डाईइलेक्ट्रिक गैसों, माइक्रोइलेक्ट्रोड फैब्रिकेशन, वेटेबिलिटी

## TABLE OF CONTENTS

<b>CERTIFICATE</b>	<b>i</b>
<b>ACKNOWLEDGEMENTS</b>	<b>ii</b>
<b>ABSTRACT</b>	<b>iv</b>
<b>सार</b>	<b>vii</b>
<b>LIST OF FIGURES</b>	<b>xv</b>
<b>LIST OF TABLES</b>	<b>xx</b>
<b>NOMENCLATURES</b>	<b>xxi</b>
<b>1. INTRODUCTION</b>	<b>1</b>
<i>1.1. Micromachining</i>	<i>1</i>
<i>1.1.1. Classification of Micromachining Processes</i>	<i>2</i>
<i>1.1.2. Electrical Discharge Machining (EDM)</i>	<i>3</i>
<i>1.1.3. Micro-Electrical Discharge Machining (<math>\mu</math>EDM)</i>	<i>4</i>
<i>1.1.4. Process Variants of <math>\mu</math>EDM</i>	<i>6</i>
<i>1.2. Need for on-machine microelectrode fabrication</i>	<i>7</i>
<i>1.3. Uses of microelectrodes</i>	<i>7</i>
<i>1.4. Microelectrode fabrication methods</i>	<i>7</i>
<i>1.4.1. Wire-based microelectrode fabrication</i>	<i>7</i>
<i>1.4.2. Disc-based microelectrode fabrication</i>	<i>9</i>
<i>1.4.3. Rod-based microelectrode fabrication</i>	<i>10</i>
<i>1.4.4. Strip-based microelectrode fabrication</i>	<i>10</i>
<i>1.4.5. Block-based microelectrode fabrication</i>	<i>11</i>
<i>1.5. Motivation for the present work</i>	<i>12</i>
<i>1.6. Organization of thesis</i>	<i>13</i>
<b>2. LITERATURE REVIEW</b>	<b>14</b>
<i>2.0. Introduction</i>	<i>14</i>
<i>2.1. Fabrication of microelectrode</i>	<i>14</i>
<i>2.1.1 The effect of non-electrical parameters in dry EDM</i>	<i>15</i>
<i>2.1.2 The effect of gaseous dielectric in dry EDM</i>	<i>18</i>
<i>2.2. Literature review on the application of microelectrodes</i>	<i>23</i>

2.2.1 <i>The wettability characteristics</i>	25
2.3. <i>Literature review on Dry <math>\mu</math>EDM setup</i>	29
2.4. <i>Research gap</i>	33
2.5. <i>Objectives of the present work</i>	33
<b>3. DESIGN AND DEVELOPMENT OF DRY <math>\mu</math>EDM SETUP</b>	<b>34</b>
3.0. <i>Introduction</i>	34
3.1. <i>Design requirements</i>	34
3.1.1 <i>Motion control</i>	36
3.1.2 <i>Pulsed power supply for dry <math>\mu</math>EDM</i>	37
3.1.3 <i>Electrically isolated EDM spindle</i>	39
3.1.4 <i>Dielectric fluid delivery system</i>	43
3.1.5 <i>In-situ metrology</i>	44
3.2. <i>Applications</i>	45
3.3. <i>Integration of Dry <math>\mu</math>EDM in Advanced Micromachining System (AMMS)</i>	47
3.4. <i>Conclusions</i>	48
<b>4. MICROELECTRODE FABRICATION USING DIFFERENT MACHINING STRATEGIES THROUGH DRY <math>\mu</math>-ED TURNING</b>	<b>50</b>
4.0. <i>Introduction</i>	50
4.1. <i>Material and methods</i>	50
4.1.1 <i>Material of rod and block electrodes</i>	50
4.1.2 <i>Experimental setup</i>	51
4.1.3 <i>Machining strategies for the fabrication of microelectrodes</i>	53
4.2. <i>Results and discussions</i>	54
4.2.1 <i>Dimensional analysis of microelectrode</i>	54
4.2.1.1 <i>Analysis of the diameter of microelectrodes</i>	55
4.2.1.2 <i>Analysis of the taper angle of microelectrodes</i>	57
4.2.2 <i>Surface morphology</i>	59
4.2.2.1 <i>SEM analysis of fabricated microelectrodes surface</i>	59
4.2.2.2 <i>SEM analysis of microelectrodes fabricated through MB-EDT<sub>d</sub> at various discharge currents</i>	61
4.2.3 <i>Surface roughness</i>	62
4.2.3.1 <i>Analysis of surface roughness of microelectrodes</i>	62

4.2.3.2	<i>Analysis of surface roughness of microelectrodes fabricated through MB-EDT<sub>d</sub> at various discharge currents</i>	63
4.3.	<i>Conclusions</i>	63
<b>5.</b>	<b>EFFECT OF NON-ELECTRICAL PARAMETERS IN THE FABRICATION OF MICROELECTRODES USING Dry <math>\mu</math>EDT</b>	<b>65</b>
5.0.	<i>Introduction</i>	65
5.1.	<i>Materials and method</i>	66
5.1.1	<i>Materials</i>	66
5.1.2	<i>Method</i>	66
5.1.3	<i>Selection of process factors</i>	67
5.2.	<i>Design of experiments</i>	68
5.2.1	<i>Statistical modelling of material removal rate and surface roughness</i>	68
5.2.2	<i>Model range prediction</i>	71
5.3.	<i>Results and discussions</i>	72
5.3.1	<i>Effect of process parameters on MRR</i>	72
5.3.1.1	<i>Effect of spindle rotation speed</i>	73
5.3.1.2	<i>Effect of block linear feed</i>	73
5.3.1.3	<i>Effect of dielectric pressure</i>	73
5.3.2	<i>Interaction effect of process parameter on MRR</i>	74
5.3.3	<i>Effect of process parameters on surface roughness</i>	75
5.3.3.1	<i>Effect of spindle rotation speed</i>	75
5.3.3.2	<i>Effect of block linear feed</i>	76
5.3.3.3	<i>Effect of dielectric pressure</i>	77
5.4.	<i>Optimization of process response using GA</i>	77
5.5.	<i>Surface morphology of fabricated microelectrodes</i>	78
5.6.	<i>Conclusions</i>	80
<b>6.</b>	<b>PERFORMANCE ASSESSMENT OF GASEOUS DIELECTRICS DURING MICROELECTRODE FABRICATION</b>	<b>82</b>
6.0	<i>Introduction</i>	82

6.1 <i>Materials and method</i>	82
6.1.1 <i>Materials</i>	82
6.1.2 <i>Method</i>	83
6.2 <i>Results and discussions</i>	85
6.2.1 <i>Geometrical analysis of microelectrodes</i>	85
6.2.2 <i>Effect of different gaseous dielectric on surface topography of Microelectrodes</i>	88
6.2.2.1 <i>Surface topography</i>	88
6.2.2.2 <i>Surface recast layer</i>	91
6.2.3 <i>Chemical composition analysis</i>	96
6.3 <i>Conclusions</i>	98
<b>7. SURFACE MODIFICATION OF Al-6061 ALLOY USING DRY <math>\mu</math>EDM MILLING</b>	<b>100</b>
7.0. <i>Introduction</i>	100
7.1. <i>Materials and method</i>	102
7.1.1 <i>Materials</i>	102
7.1.2 <i>Method</i>	102
7.2. <i>Results and discussions</i>	104
7.2.1 <i>Morphology and topography</i>	104
7.2.2 <i>Surface wettability and contact angle measurement</i>	106
7.2.3 <i>Surface chemical analysis</i>	109
7.2.3.1 <i>EDAX analysis</i>	109
7.2.3.2 <i>XRD analysis</i>	111
7.2.3.3 <i>XPS analysis</i>	113
7.3. <i>Conclusions</i>	118
<b>8. CONCLUSIONS AND SCOPE OF FUTURE WORK</b>	<b>119</b>
8.0. <i>Conclusions</i>	119
8.1. <i>Summary of major contributions</i>	123
8.2. <i>Scope of future work</i>	124
<b>References</b>	<b>125</b>

<b>Appendix – A</b>	<b>137</b>
Technical specifications of programmable DC power supply	
<b>Appendix – B</b>	<b>139</b>
Wiring diagram of the pulse generator	
<b>Appendix – C</b>	<b>147</b>
2D drawings of EDM spindle (third version)	
<b>Appendix – D</b>	<b>155</b>
2D drawings of EDM spindle (fourth version)	
<b>Appendix – E</b>	<b>162</b>
Microhole dry $\mu$ EDM drilling	
<b>PUBLICATIONS AND AWARDS</b>	<b>164</b>
<b>AUTHOR BIOGRAPHY</b>	<b>166</b>

# LIST OF FIGURES

Fig. 1.1	Classification of micromachining processes based on the type of energy used for material removal	2
Fig. 1.2	General principle of EDM	3
Fig. 1.3	Graphical explanation of spark formation and material removal in $\mu$ EDM	4
Fig. 1.4	Comparison between crater dimensions in (a) conventional EDM, and (b) $\mu$ EDM	5
Fig. 1.5	Classification of microelectrode manufacturing process for $\mu$ EDM, based on the shape of the tool electrode	7
Fig. 1.6	Comparison between radial and tangential feed WEDG (a) WEDG construction; (b) radial feed WEDG; (c) tangential feed WEDG	8
Fig. 1.7	Twin-wire EDM system for micro tool fabrication	9
Fig. 1.8	Rotating sacrificial disk	9
Fig. 1.9	Principle of fabricating microelectrodes	10
Fig. 1.10	(a) Schematic of the design and components used; (b) process of strip EDM turning	11
Fig. 1.11	Schematic of (a) stationary block EDT (SB-EDT), and (b) moving block EDT (MB-EDT)	12
Fig. 2.1	Relative motion between tool and workpiece in various EDM variants to fabricate different shapes	15
Fig. 2.2	Microscopic images of a fabricated microelectrode showing tip and root	16
Fig. 2.3	Schematic of the block- $\mu$ EDM process without moving block (a) before; (b) after the microelectrode fabrication	17
Fig. 2.4	Schematic of the block- $\mu$ EDM process with moving block (a) before; (b) after the microelectrode fabrication	17
Fig. 2.5	Environmental effect of EDM/WEDM	19
Fig. 2.6	Surface topography of the workpiece machined in different dielectrics (a) argon; (b) nitrogen; (c) oxygen	20
Fig. 2.7	SEM micrographs of machined surfaces in different machining conditions (a) without air; (b) air-assisted; (c) argon gas-assisted	22
Fig. 2.8	(a) MRR variation of micro holes; (b) hole overcut with discharge energy	23
Fig. 2.9	SEM micrographs of the micro holes drilled in different dielectric mediums (a) deionized water; (b) oxygen; (c) argon	24

Fig. 2.10	Tip morphology of microelectrode (a) before drilling; (b) after drilling	24
Fig. 2.11	Schematic of forces balancing a water drop on a textured surface	25
Fig. 2.12	SEM micrographs of crater edges at different magnifications created by sinking EDM (a, b) crater generated at higher discharge energy, (c, d) crater edges reduced by lower discharge energy	27
Fig. 2.13	Comparison of C/Al and C-C(H)/Al ratios of the surface machined in different dielectrics	27
Fig. 2.14	Photograph of droplet shape and CA (a); (b) before and (c); (d) after machining	27
Fig. 2.15	Schematic representation of hydrophobic generation process with different machining conditions (a) rough step; (b) finished surfaces; (c) SEM images of the surface generated in four machining cuts	28
Fig. 2.16	Photograph of a water droplet on the surface kept in an air atmosphere	29
Fig. 2.17	Impact of different atmospheres on the contact angle of the machined surface for 30 days	29
Fig. 2.18	Atomic ratio C/Al on the machined surface kept in a different atmosphere	29
Fig. 2.19	Available industrial CNC EDM centers (a) Sodick K4HL; (b) Sarix MACHLine; (c) ONA micro hole EDM; (d) Mitsubishi SG8	30
Fig. 2.20	Lab scale dry EDM experimental setup (a) schematic; (b) photograph	31
Fig. 2.21	Lab scale dry EDM experimental setup (a) schematic; (b) photograph	31
Fig. 2.22	Modified dry EDM experimental setup	32
Fig. 2.23	(a) Integrated nano grinding center; (b) Integrated DT-110 machine tool	32
Fig. 3.1	Schematic of Dry $\mu$ EDM setup	35
Fig. 3.2	Photograph of the dry $\mu$ EDT setup	35
Fig. 3.3	Schematics of connection diagram between Controller, Drive, Servomotor, and PC	36
Fig. 3.4	Connection diagram of the pulse generator with linear slide, tool, and workpiece	37
Fig. 3.5	Photograph of the pulse generator	39
Fig. 3.6	First version of the spindle driven by the motor using a timing belt	40
Fig. 3.7	Second version of the spindle driven by the motor using a gear arrangement	40
Fig. 3.8	CAD model and photograph of the third version EDM spindle	41

Fig. 3.9	Photograph of (a) angular contact ceramic ball bearing; (b) flexible jaw coupling; (c) carbon brush	41
Fig. 3.10	CAD model and photograph of the fourth version EDM spindle	43
Fig. 3.11	Screenshot of motion control and camera software used for block and rod alignment in dry $\mu$ EDT setup	44
Fig. 3.12	Type of alignment errors: (a) Tip contact; (b) Collar contact; (c) Normal contact	45
Fig. 3.13	Different stages of microelectrode fabrication (a) Rough; (b) Semi-finish; (c) Finish operation	45
Fig. 3.14	Microscopic images of fabricated microelectrodes using dry $\mu$ EDT setup	46
Fig. 3.15	Dry $\mu$ EDT setup integrated with laser and High-speed spindle	47
Fig. 3.16	Developed AMMS system	48
Fig. 4.1	Pictorial view of dry $\mu$ EDM setup	52
Fig. 4.2	Schematics of (a) Stationary Block EDT (SB-EDT); (b) Moving Block EDT (MB-EDT)	52
Fig. 4.3	Optical microscopic images of microelectrodes after finishing operation (a) SB-EDT <sub>s</sub> , (b) MB-EDT <sub>s</sub> , (c) SB-EDT <sub>d</sub> , MB-EDT <sub>d</sub> , (e) Hybrid BEDT	55
Fig. 4.4	SEM images of block electrode used in (a) SB-EDT; (b) MB-EDT	56
Fig. 4.5	(a) Taper angle of fabricated microelectrodes; (b) MRR, and average diameter for five fabricated microelectrodes	58
Fig. 4.6	SEM micrographs of microelectrodes surface (a) SB-EDT <sub>s</sub> , (b) SB-EDT <sub>d</sub> , (c) MB-EDT <sub>s</sub> , (d) MB-EDT <sub>d</sub> , (e) Hybrid BEDT, and (f) position on the microelectrode where SEM was performed	60
Fig. 4.7	SEM micrographs of the surface of microelectrodes (a) MB-EDT <sub>d</sub> at 3A; (b) MB-EDT <sub>d</sub> at 4A; (c) MB-EDT <sub>d</sub> at 5A	61
Fig. 4.8	Average surface roughness of microelectrodes fabricated through different machining strategies	62
Fig. 5.1	Schematic diagram of MB-EDT process (a) before the start of machining; (b) after machining with block wear and fabricate microelectrode	66
Fig. 5.2	Optical images of fabricated microelectrodes	67
Fig. 5.3	(a) Main effect plot; and (b) percentage of factor contribution on MRR	72

Fig. 5.4	The interaction effect between spindle rotation speed and dielectric pressure on MRR, (a) response surface for MRR; (b) variation of MRR with spindle rotation speed and dielectric pressure	74
Fig. 5.5	The interaction effect between block linear feed and dielectric pressure on MRR, (a) response surface for MRR; (b) variation of MRR with block linear feed and dielectric pressure	75
Fig. 5.6	(a) Main effect plot, and (b) percentage of factor contribution on surface roughness	76
Fig. 5.7	SEM micrographs of fabricated microelectrodes at process factors	79
Fig. 6.1	Schematic of steps followed for microelectrode fabrication	84
Fig. 6.2	Optical images of microelectrodes fabricated in (a) oxygen; (b) argon; (c) compressed air; (d) compressed air-argon; (e) oxygen-argon; (f) nitrogen	86
Fig. 6.3	Schematics of the discharge channel in dielectric (a) oxygen and (b) oxygen-argon	87
Fig. 6.4	Variation in diameter reduction during three machining cuts in various dielectrics	87
Fig. 6.5	Variation in surface roughness during three machining cuts in various dielectrics	88
Fig. 6.6	SEM micrographs (at 1000x magnification) of microelectrodes surface machined by rough cut in different dielectrics	89
Fig. 6.7	SEM micrographs (at 1000x magnification) of microelectrodes surface machined by a semi-finish cut in different dielectrics	90
Fig. 6.8	SEM micrographs (at 1000x magnification) of microelectrodes surface machined by finish cut in different dielectrics	90
Fig. 6.9	(a) XMCT 3D image of microelectrode fabricated in compressed air; (b) cross-sectional view at different heights; (c) 3D reconstructed volume image of the sample at different angles	92
Fig. 6.10	3D volume images viewed from different angles (a) finish cut length; (b) semi-finish cut length; (c) rough cut length	93
Fig. 6.11	Optical images of various sections machined through rough, semi-finish, and finish cut after etching	94
Fig. 6.12	SEM micrograph (at 200x magnification) of recast layer thickness in microelectrode fabricated in oxygen-argon dielectric	94

Fig. 6.13	Recast layer thickness of microelectrodes fabricated in various dielectrics	95
Fig. 6.14	EDAX analysis of microelectrodes surface fabricated in different dielectrics (a) unmachined brass rod; (b) oxygen; (c) compressed air; (d) nitrogen; (e) compressed air-argon; (f) oxygen-argon; (g) argon	97
Fig. 7.1	$\mu$ EDM milling schematics of (a) process and (b) tool path movement	102
Fig. 7.2	Schematics of the craters created on the Al-6061 alloy surface during (a) rough cut; (b) semi-finish cut; (c) finish cut	104
Fig. 7.3	SEM micrographs (1,3,5) and three-dimensional surface topographies (2,4,6) of the polished and modified surfaces of Al-6061 alloy in oxygen and argon gases	105
Fig. 7.4	Schematic of the forces on the droplet and surface topography of (a) sample machined in oxygen gas and (b) sample machined in argon gas	108
Fig. 7.5	Measured static contact angle on the aluminum surface before machining, after machining, and after 30 days of machining	108
Fig. 7.6	Graph of contact angle variation with the date (a) aluminum machined in oxygen gas dielectric; (b) aluminum machined in argon gas dielectric	109
Fig. 7.7	EDAX results for samples of (a) unmachined Al-6061 alloy; (b) machined in oxygen, and (c) machined in argon	110
Fig. 7.8	XRD results of the polished unmachined sample after machining and 30 days after machining in oxygen gas dielectric	112
Fig. 7.9	XRD results of the polished unmachined sample after machining and 30 days after machining in argon gas dielectric	112
Fig. 7.10	XPS spectra for (a) the polished surface of Al-6061 alloy before machining; (b) after machining in oxygen dielectric; (c) after machining in argon dielectric, and (d) the atomic ratio of C/Al on the surface as determined by high-resolution XPS spectra	114
Fig. 7.11	XPS spectra for Al 2p peaks for (a) the polished surface of Al-6061 alloy before machining; (b) after machining in oxygen dielectric; (c) after machining in argon dielectric, and (d) combined Al 2p peaks of all samples	116
Fig. 7.12	XPS spectra for C 1s peaks for (a) the polished surface of Al-6061 alloy before machining; (b) after machining in oxygen dielectric; (c) after machining in argon dielectric, and (d) combined C 1s peaks of all samples	117

## LIST OF TABLES

Table 1.1	Difference between $\mu$ EDM and macro EDM	5
Table 3.1	Technical specification of the pulse generator	38
Table 4.1	Chemical composition of Brass IS 319 Gr. 1	51
Table 4.2	Physical properties of workpiece/tool material	51
Table 4.3	Description and schematic of five machining strategies used for microelectrode fabrication	53
Table 4.4	Machining parameters for fabricating microelectrodes	54
Table 5.1	Fixed process factors for rough and finish machining cut	67
Table 5.2	Parameters for fabricating electrodes illustrated in Fig. 5.2	67
Table 5.3	Selected process factors and their levels	68
Table 5.4	Experimental runs and measured process responses	69
Table 5.5	ANOVA table for measured MRR	70
Table 5.6	ANOVA table for measured $R_a$	70
Table 5.7	Validation experimentation for the developed model	71
Table 5.8	The optimized parameters for MRR and $R_a$	78
Table 6.1	Thermal and physical properties of dielectric gases at 25 °C	83
Table 6.2	Dry $\mu$ EDM process parameters	84
Table 6.3	Parameters for performing XMCT	92
Table 7.1	Machining parameters used for Al 6061 surface modification	103
Table 7.2	Chemical composition of Aluminum-6061 alloy before and after machining in oxygen and argon dielectric	110

# NOMENCLATURES

AMMS	Advanced Micromachining System
MEMS	Microelectromechanical Systems
EDM	Electric Discharge Machining
$\mu$ EDM	Micro Electric Discharge Machining
$\mu$ EDT	Micro Electric Discharge Turning
$\mu$ EDG	Micro Electric Discharge Grinding
WEDG	Wire Electric Discharge Grinding
TF-WEDG	Tangential Feed Wire Electric Discharge Grinding
CCD	Central Composite Design
ANOVA	Analysis of Variance
GA	Genetic Algorithm
TrC	Transistor Electro Discharge Circuit
RC	Resistance Capacitance Electro Discharge Circuit
DC	Direct Current
IEG	Inter Electrode Gap
BEDT	Block Electric Discharge Turning
SB-EDT	Stationary Block Electric Discharge Turning
MB-EDT	Moving Block Electric Discharge Turning
MOSFET	Metal-Oxide-Semiconductor Field-Effect Transistor
MRR	Material Removal Rate
$R_a$	Average Surface Roughness
RLT	Recast Layer Thickness
CA	Contact Angle
SEM	Scanning Electron Microscope
EDAX	Energy Dispersive X-Ray Analysis
XRD	X-Ray Diffraction
XPS	X-Ray Photoelectron Spectroscopy